Published in final edited form as:
Aging Cell. 2013 August ; 12(4): 672–681. doi:10.1111/acel.12091.

A shift in energy metabolism anticipates the onset of sarcopenia in rhesus monkeys

Thomas D. Pugh[1], **Matthew W. Conklin**[2], **Trent D. Evans**[1], **Michael A. Polewski**[1], **Hannah J. Barbian**[1], **Rachelle Pass**[1], **Bradley D. Anderson**[1], **Ricki J. Colman**[3], **Kevin W. Eliceiri**[2], **Patricia J. Keely**[4], **Richard Weindruch**[1,5], **T. Mark Beasley**[6], and **Rozalyn M. Anderson**[1,3,5]

Thomas D. Pugh: tdpugh@wisc.edu; Matthew W. Conklin: mwconklin@wisc.edu; Trent D. Evans: trent.evans@colorado.edu; Michael A. Polewski: mapolewski@wisc.edu; Hannah J. Barbian: hbarbian@mail.med.upenn.edu; Rachelle Pass: rachellepass@uwalumni.com; Bradley D. Anderson: bdanderson@wisc.edu; Ricki J. Colman: rcolman@primate.wisc.edu; Kevin W. Eliceiri: eliceiri@wisc.edu; Patricia J. Keely: pjkeely@wisc.edu; Richard Weindruch: rhweindr@wisc.edu; T. Mark Beasley: MBeasley@ms.soph.uab.edu

[1]Department of Medicine, University of Wisconsin, Madison WI 53706

[2]Laboratory for Optical and Computational Instrumentation, University of Wisconsin, Madison WI 53706

[3]National Primate Research Center, University of Wisconsin, Madison WI 53715

[4]Department of Cell and Regenerative Biology, University of Wisconsin, Madison 53706

[5]GRECC, William S. Middleton Memorial Veterans Hospital, Madison WI, 53705

[6]Department of Biostatistics, University of Alabama, Birmingham AL 35294

Summary

Age-associated skeletal muscle mass loss curtails quality of life and may contribute to defects in metabolic homeostasis in older persons. The onset of sarcopenia occurs in middle age in *rhesus macaques* although the trigger has yet to be identified. Here we show that a shift in metabolism occurs in advance of the onset of sarcopenia in rhesus *vastus lateralis*. Multiphoton laser scanning microscopy detects a shift in the kinetics of photon emission from autofluorescent metabolic cofactors NADH and FAD. Lifetime of both fluorophores is shortened at mid-age and this is observed in both free and bound constituent pools. Levels of FAD and free NADH are increased and the NAD/NADH redox ratio is lower. Concomitant with this, expression of fiber type myosin isoforms is altered resulting in a shift in fiber type distribution, activity of cytochrome c oxidase involved in mitochondrial oxidative phosphorylation is significantly lower, and the sub-cellular organization of mitochondria in oxidative fibers is compromised. A regulatory switch involving the transcriptional coactivator PGC-1α directs metabolic fuel utilization and governs the expression of structural proteins. Age did not significantly impact total levels of PGC-1α; however, its sub-cellular localization was disrupted, suggesting that PGC-1α activities may be compromised. Consistent with this, intracellular lipid storage is altered and there is shift to larger lipid droplet size that likely reflect a decline in lipid turnover or a loss in efficiency of lipid metabolism. We suggest that changes in energy metabolism contribute directly to skeletal muscle aging in rhesus monkeys.

Keywords

Aging; metabolism; NAD; mitochondria; PGC-1α; skeletal muscle; rhesus monkeys

Corresponding author Rozalyn M. Anderson, GRECC D5214, VA Hospital, 2500 Overlook Terrace, Madison, WI 53705. Phone: 608 256 1901 x 11591, Fax: 608 280 7291, rmanderson@medicine.wisc.edu.

Introduction

As a model for human aging, the rhesus monkey (*Macaca mulatta*) provides several strengths including a high degree of genetic identity to humans, a lifespan of several decades, and a spectrum of age-associated diseases that mirror those in humans (Uno 1997). Sarcopenia is the age-associated decline in muscle mass. The kinetics of muscle mass loss in rhesus monkeys is similar to that of humans. Rhesus monkeys have an average lifespan of ~ 27 years, the process of sarcopenia occurs gradually with onset in middle age at ~15 years of age (Colman *et al.* 2005; McKiernan *et al.* 2009). The physical basis for the disorder is thought to be a combination of atrophy and loss of the constituent muscle fibers. Several studies have noted defects in energy metabolism in skeletal muscle from older humans, rats, and mice (Proctor *et al.* 1995; Figueiredo *et al.* 2009; Noland *et al.* 2009). These findings are corroborated by meta-analysis of gene expression studies that demonstrate that the expression of genes involved in mitochondrial electron transport system is lower in aged tissues (Mootha *et al.* 2003; Zahn *et al.* 2006; de Magalhaes *et al.* 2009). What is not yet clear is whether changes in energy metabolism are symptomatic late events in sarcopenia or causative events that contribute to age-dependent vulnerability for muscle mass loss.

The cellular composition of skeletal muscle is heterogeneous. Individual muscle fibers differ in the isoform of the structural protein myosin that is expressed and in whether oxidative or non-oxidative metabolism is favored (Bassel-Duby & Olson 2006). Slow twitch oxidative fibers express the Type I myosin isoform and are associated with endurance. Fast twitch fibers are thought to be more dependent on glycolytic energy metabolism, express Type II myosin isoform and are associated with greater strength and force. Metabolic genes and myosin isoform expression are coordinately regulated through the transcriptional coactivator PGC-1α (PPAR gamma coactivator 1 alpha) (Lin *et al.* 2002). The heterogeneity of fiber composition can present a challenge in elucidating the impact of age on skeletal muscle because the response of individual fiber types is not equivalent. We and others have shown that Type II fibers are vulnerable to age-associated atrophy in humans and in nonhuman primates while Type I fibers generally are not (Lexell 1995; Proctor *et al.* 1995; McKiernan *et al.* 2009). These data suggest that fibers of distinct structural and metabolic profiles are differentially impacted by age.

Here we use a quantitative intrinsic fluorescence imaging based approach that allows differences among fiber types to be determined as a function of age. The impact of aging on muscle metabolism in primates and how it relates to the onset of muscle mass loss has not been well characterized. In humans, defects in skeletal muscle energy metabolism are linked to glucoregulatory dysfunction (Petersen *et al.* 2004) and type 2 diabetes (Lowell & Shulman 2005), indicating that changes in muscle metabolism can have systemic effects. In this way, the decline in skeletal muscle mass with age could have ramifications for whole body metabolic homeostasis. The goal of this study was to understand what leads to sarcopenia onset.

Results

Altered photon kinetics of cofactors NADH and FAD are indicative of a shift in metabolism in mid-age

We investigated the impact of age on metabolism in rhesus monkey *vastus lateralis* (VL). We focused on three age groups: young adults of full stature (age 6–9 years), mid-age animals at the time of onset of sarcopenia but prior to muscle mass loss (age 15–16 years), and old age (age 28–32 years) where sarcopenia is already well established. Postmortem analysis of quadriceps muscles shows the extent of sarcopenia among these selected age

groups (Supplementary Table 1). Of the four constituent muscle groups within the quadriceps the VL is most vulnerable to age. VL from old animals weighed significantly less than those of young animals (39%), and weights of muscles from young and middle age animals are not different. Age was significantly related to VL ($p= 0.0403$) with VL reducing by 1.435 units per year (95% CI: −2.796 to −0.075) between middle age and old age. As a complementary analysis the degree of fibrosis was assessed histologically in tissue sections from the study cohort. One of the compensatory adaptations to fiber atrophy with sarcopenia is that gaps between and around fibers become filled with fibrotic material. Quantitative analysis of fiber and non-fiber area within the muscle tissue sections revealed no difference between the young and mid-age animals (Supplementary Table 2). In contrast, tissue sections from old animals showed a significant degree of fibrosis (15% total area), in agreement with previously published data on similarly aged monkeys (McKiernan *et al.* 2012).

To gain a comprehensive metabolic perspective we employed two complementary imaging methods: multiphoton laser-scanning microscopy (MPLSM) (Denk *et al.* 1990; Zipfel *et al.* 2003; Skala *et al.* 2007), and fluorescent lifetime microscopy (FLIM) (Lakowicz *et al.* 1992), that when utilized together can uniquely probe intrinsic fluorescent properties of metabolites. Using these techniques differences in metabolism at the individual cell level can be inferred. The cofactors NAD^+/NADH and FAD/$FADH_2$ play an integral role in metabolism. Due to innate autofluorescent properties of reduced and oxidized forms respectively, NADH and FAD can be monitored directly and nondestructively in individual cells or tissue sections using optical sectioning high-resolution microscopy techniques. Single photon absorption of NADH and FAD spans the UV and visible spectrum and the emission spectra are partially overlapping (Figure S1). Multiphoton laser-scanning microscopy is effective for the detection and discrimination of NADH and FAD (Skala *et al.* 2007). This approach utilizes two different excitation wavelengths and involves a spectral separation of the emission signals (Bird *et al.* 2004). Photon emission at 890nm excitation wavelength is predominantly due to the autofluoresence of FAD. At 780nm, both FAD and NADH emit but the contribution from NADH is greater (Figure S1) and FAD and NADH can be separated through gating of the excitation wavelength. FLIM detects changes in the fluorescent lifetime, the duration that the fluorophore stays in the excited state (Yan *et al.* 2006). For each specimen the fluorescent decay curve was generated over multiple pulses and repeated for each pixel in the image capture field. The lifetime curve fits as the sum of two exponentials; a short component τ_1 and a long component τ_2 that represent distinct states of the fluorophore. The weighted average (τ_m) of both components is expressed in picoseconds and color-coded to allow differences among fibers to be visualized (Figure 1).

In muscle sections from young animals three distinct fiber type populations were detected based on the lifetime calculation for FAD and NADH. This gives rise to a checkerboard pattern in the color-map image of bright green (longest τ_m), dark green shortest τ_m), and intermediate fibers (Figure 1A). There was agreement among the categories for images generated at 890nm and 780nm excitation indicating the photon kinetics of both fluorophores were similar and characteristic of that fiber type. In mid-age specimens distinct fiber populations were also identified; however, the lifetime was shifted to more rapid decay in each fiber type category and for both fluorophores. For FAD, the short component represents bound cofactor where protein binding quenches the excited state while the free cofactor is represented by the long component (Tanaka *et al.* 1989). The opposite is the case for NADH; the stacking of the nicotinamide ring with the adenine moiety results in self-quenching such that the free cofactor is represented as the short component and the bound cofactor is the long component (Lakowicz *et al.* 1992). Photon emission properties in mid-age tissues were significantly shorter ($p<0.05$) for both τ_1 and τ_2 decay components (Figure 1B). In tissues from old animals the lifetime is shifted again to longer duration lifetime for

both fluorophores. The properties of photon emission are influenced by local environment including subcellular localization, oxidative or hypoxic conditions, and the identity of proteins to which they are bound. These data demonstrate that the intracellular environment is altered with age and indicate that a shift in metabolism occurs in advance of the onset of sarcopenia.

Two additional features were identified using this imaging technique. The first, which appeared in the image as red strings, is generated by hydroxylysyl pyridiniline and lysyl pyridinoline crosslinks in collagen, and was more prevalent in tissues from old animals. The photons emitted were sufficiently distinct that they could be excluded from the lifetime calculation. The second source was visualized as blue dots. The size and intensity of the dots are exaggerated by the processing of the image where thousands of photons are binned across pixels. These were also more prevalent in old specimens with the result that the change in the lifetime from mid-age to old is likely to be underestimated.

NADH availability and NAD:NADH redox changes occur in advance of the onset of sarcopenia

The fluorescence lifetime provides information about the chemical microenvironment and binding state of fluorophores in the cell but is not a measure of fluorophore concentration (Lakowicz *et al.* 1992). To determine whether differences in photon kinetics among fibers are associated with differences in levels of cofactors we measured the intensity of fluorescence using MPSLM at both 890nm and 780nm excitation wavelengths (Figure 2A, Figure S2). In sections from young animals three fiber types were clearly identified based on the intensity of fluorescence: bright, mid-level brightness, and low intensity. Overall fluorescent intensity at excitation of 890nm was greater in tissues from mid-age animals compared to young animals (Figure 2B), but the intensity within individual fibers from the brighter categories was lower and the contrast among fiber types diminished. In tissues from old animals the difference in intensity among fibers was less clear and overall fluorescent intensity was lower. At excitation of 780nm we did not detect a significant difference in fluorescent intensity with age although values for mid-age animals tended to be higher than for young or old animals.

In addition to the dispersed autofluorescence attributed to FAD and NADH, a population of small bright foci were detected exclusively in tissues from old animals. The excitation parameters indicate that they are most likely to be lipofuscin (Bindewald-Wittich *et al.* 2006), lipid containing lysosomal remnants that are associated with aging. A comparison with the lifetime imaging indicated that for old animals the bright foci colocalized with the blue dots described previously and may explain the increased prevalence of blue dots in the specimens from old animals (Figure 1A, 2A). These findings indicate that the source of the blue dots in the lifetime images for old animals is lipofuscin, whereas the blue dots observed in the young and middle-aged animals are a result of the binning process in areas of high fluorescent intensity around the cell periphery.

One critical aspect of these analyses is that the oxidized form of FAD is detected but for NAD, the reduced form is detected. In this way the fact that age impacts FAD but not so much NADH may reflect a redox shift in mid-age. To test this we used a biochemical approach where NADH is detected using an enzyme linked assay. There are two important caveats to consider, first the assay utilizes tissue homogenate so that differences among fiber types cannot be distinguished and second, the purification steps taken to ensure the integrity of the redox state within the specimens exclude the bound populations of NAD and NADH and measure only what is free. We identified a significant increase in NADH in tissues from mid-age animals compared to young animals and a subsequent decline in the older specimens, suggesting that there is a change in availability of NADH with age independent

of total NADH pools (Figure 2C). In addition we detected a change in ratio of the free NAD and NADH populations, indicating that a redox shift occurs as animals enter mid-age (Figure 2C).

Changes in muscle fiber structural protein expression occur at mid-age prior to the onset of sarcopenia

The fibers that make up skeletal muscle are heterogeneous and differ mechanically and metabolically (Bassel-Duby & Olson 2006). Approaches used to categorize fiber types take advantage of differences in the isoform of the structural protein myosin or the optimal pH of the myofibrillar associated ATPase. Immunohistological detection in serial sections of VL using antibodies specific to Type I or Type II myosin isoforms identifies 3 classes of fibers: pure Type I, pure Type II, and mixed myosin fibers (MMF) that express both myosin isoforms (Figure 3A, marked a, b, c respectively). In animals from the young group, the predominant fiber type is the hybrid MMF, with pure Type I and pure Type II fibers making up only ~20% of the total population (Figure 3B, Supplemental Table 3). By mid-age, the fiber type distribution has shifted significantly with roughly equal proportions of the 3 fiber types. In the old animals the classic phenotypes of sarcopenia were observed, including increased fibrosis, a tendency for centralized nuclei, and the emergence of clusters of same-type fibers. The overall fiber-type distribution in old animals, however, is not different from that of mid-age animals showing that a reduction in the proportion of fibers with dual structural protein isoform expression occurs in advance of the onset of sarcopenia.

To confirm that the shift in fiber type distribution is an age effect rather than a late developmental effect, we investigated fiber type distribution monkeys on the anti-aging regimen of caloric restriction (CR). We have previously shown that CR promotes survival in rhesus monkeys and attenuates the onset of multiple age-associated diseases and disorders (Colman *et al.* 2009), including sarcopenia (McKiernan *et al.* 2011; McKiernan *et al.* 2012). In old CR animals the fiber type distribution was significantly different from that of Control fed animals with MMF being the predominant fiber type (Figure 3C). This profile is reminiscent of the distribution in normally fed young animals and suggests that the shift in fiber type composition that we detect at mid-age is indeed an aging phenotype.

To assess the impact of age on fiber atrophy the cross-sectional area (CSA) was measured for each fiber type at each of the three age groups (Figure 3D, Supplemental Table 4). As might be expected based on the muscle wet weight measures, the CSA for each fiber type was not different between young and mid-age animals. In old animals, pure Type I fibers did not exhibit significant atrophy with age; however, the CSA of fibers expressing Type II myosin isoforms was lower in older animals. The pure Type II fibers were most vulnerable to the impact of age with significantly smaller CSA (34% reduction) in old muscle compared to young animals and mid-age animals. In the MMF fibers, while the CSA tended to be smaller in old animals, the impact of age was not as striking (14% reduction) and did not reach significance.

Using multiphoton scanning microscopy we identified three fiber types that differed both in their NADH and FAD photon kinetics and in the intensity of autofluorescence. By comparison of adjacent sections we determined that the long τ_m, bright fluorescence fibers were pure Type I myosin expressing fibers, the short τ_m, low level fluorescence fibers were MMF, and the intermediate fibers were pure Type II. The change in fiber type composition with age may be a contributing factor in the increase in autofluorescence identified in mid-age animals (proportionally more Type I and pure Type II) but does not explain the shift in photon kinetic properties (towards shorter τ_m) or in NAD:NADH redox.

Mitochondrial metabolism and subcellular organization is progressively compromised with age

An alternate system of muscle fiber type classification considers the metabolic properties of the fibers distinguishing between oxidative (slow twitch) and glycolytic (fast twitch) fibers (Zierath & Hawley 2004). To determine whether the changes observed in fluorescent lifetime at mid-age were coincident with changes in mitochondrial activity and how both of these measures related to fiber type (as characterized by myosin isoform expression) we used a histochemical approach. Cytochrome c oxidase enzymatic activity is exclusive to Complex IV of the mitochondrial electron transport system (ETS) that is required for oxidative phosphorylation. Differences among heterogeneous cell populations can be quantitatively measured using the cytochrome c oxidase activity stain, a technique that measures maximal enzymatic activity (Seligman *et al.* 1968). As expected, mitochondrial activity stain intensity was highest for pure Type I fibers. Somewhat unexpectedly, pure Type II fibers stained with greater intensity than Type I/Type II hybrid MMFs, indicating that mitochondrial oxidative capacity is higher in the pure fiber type (Figure 3E, Supplemental Table 5). The age-associated shift in composition could be a result of fiber type transition, where fibers that in young express both myosin isoforms convert to pure type fibers around mid-age. In support of this concept, we identified MMF with high oxidative capacity in young and mid-age groups (Figure 3A, indicated by arrow) but not in the old animals.

The impact of age on cytochrome c oxidase activity staining was fiber type specific (Figure 3E). Type I fiber staining intensity differed significantly across age groups and pairwise comparisons indicated Type I fibers from young animals were significantly different from those of mid-age animals (Supplemental Table 5). In contrast, Type I fibers from mid-age and old animals were not different from each other. Type II fiber intensity also differed significantly across age groups, again the fibers from young animals were different from the mid-age and old animals, which were not different from each other. Cytochrome c oxidase activity stain intensity did not differ significantly across age groups for MMF indicating that these fibers are refractory to the impact of age. These changes in mitochondrial activity stain indicate that Type I and Type II fibers from young animals are not metabolically equivalent to the same fiber types in mid-age and old animals.

To determine whether the decline in mitochondrial activity with age was associated with a change in mitochondrial density or mitochondrial complexes (or both) we measured the levels of voltage dependent anion channel (VDAC) mitochondrial membrane protein and cytochrome c oxidase subunit IV in tissue homogenates from each age group (Figure 4). Notwithstanding the degree of heterogeneity conveyed by the fact that the animals in the cohort are not related, levels of VDAC and cytochrome c oxidase subunit IV were not different from young, mid-age and old animals indicating that mitochondrial density was not impacted by age. Within individual fibers in tissue sections the VDAC stain mirrored the mitochondrial activity stain to the extent that the higher capacity fibers have greater VDAC stain intensity. The reduction in mitochondrial activity stain intensity at mid-age is not explained by changes in levels of mitochondrial proteins, indicating that there is a change in mitochondrial function rather than mitochondrial density prior to the onset of sarcopenia.

In oxidative fibers from young animals, the mitochondrial stain was more intense at the cell periphery adjacent to the sarcolemma (Figure 4C, Supplemental Table 6). Previous studies in human skeletal muscle have shown that cytochrome c oxidase activity is significantly higher in subsarcolemmal mitochondria compared to intermyofibrillar mitochondria (Federico *et al.* 1987). Activity stain intensity was measured in individual pixels across individual fibers for each age group. Peaks corresponding to each periphery and two equidistant intervening points were identified and measured. As was observed for whole

fiber analysis, the mean intensity differed significantly across age groups ($p<0.01$). In addition there was a significant difference across regions, with mid-fiber activity stain intensities consistently lower than perimeter measures ($p<0.01$). The perimeter to mid-fiber intensity difference declined significantly with age ($p<0.01$), where the edge effect was greater in fibers from young animals than either mid-age or old animals (Figure 4D). These data confirm that activity of mitochondria is spatially regulated in rhesus muscle fibers and that the ability to maintain subcellular organization is lost with age. Furthermore, mitochondria with highest cytochrome c oxidase activity located at the periphery of the fiber are vulnerable to age-associated decline while the intermyofibrillar mitochondria with lower complex IV activity are more resistant to age effects.

Age impacts levels and subcellular distribution of regulators of mitochondrial energy metabolism

Most of the genes involved in mitochondrial energy metabolism are nuclear-encoded and their expression is regulated by a suite of transcription factors downstream of the transcriptional coactivator PGC-1α (Wu *et al.* 1999). PGC-1α also directs the expression of fiber type-specific genes including myosin isoform expression (Lin *et al.* 2002). We have detected an age-induced shift in both structural and metabolic profiles of muscle fibers, suggesting a role for PGC-1α in the process. Western blot of tissue homogenates did not detect a significant age effect on PGC-1α protein levels (Figure 5A). Levels of the PGC-1α activator AMPK (Jager *et al.* 2007) were lower in tissues from old animals, but the difference between young and mid-age was not significant. Levels of GSK3β, a component of insulin signaling that regulates glycogen synthesis in muscle (Sethi & Vidal-Puig 2007), and a regulator of PGC-1α stability and turnover (Anderson *et al.* 2008), were also significantly lower in old animals, though the effect was modest. NAMPT (nicotinamide phospho-ribosyltransferase) is a key enzyme in the NAD salvage pathway that influences NAD turnover and availability (Revollo *et al.* 2004). NAMPT indirectly positively impacts PGC-1α activity in skeletal muscle (Costford *et al.* 2009). Levels of NAMPT were significantly lower in tissue from old animals. These data are consistent with the lower mitochondrial activities detected in old animals but do not explain the changes in fiber type distribution and mitochondrial activity in mid-age prior to sarcopenia onset.

Immunohistochemical detection of PGC-1α in tissue sections (Figure 5B) identified PGC-1α throughout the cytosol and in foci that were confirmed to be nuclei in hematoxylin and eosin (H&E) counter-stained sections. Although the PGC-1α nuclear stain intensity tended to be greater in fibers from young animals, there was not a statistically significant difference across age groups (Figure 5C, Supplementary Table 7). The size of the PGC-1α foci increased significantly with age even though there was no impact on the size of nuclei identified using H&E stain (Figure 5D, Figure S3). There was a significant shift in focal area distribution for PGC-1α that was not observed in H&E stained sections (Figure 5E, Figure S3). The increase in focal size indicates that a pool of PGC-1α is localized just outside the nucleus in aged tissues, suggesting that the ability of PGC-1α to be sequestered in the nucleus diminishes with age. These data suggest that PGC-1α activity may be compromised with age through differential cellular localization.

Age-associated change in intracellular lipid storage suggests a shift in lipid utilization in skeletal muscle

Another important aspect of PGC-1a function in skeletal muscle is to regulate fatty acid oxidation and lipid fuel utilization (Koves *et al.* 2005). Intracellular lipids are stored in droplets, the size and distribution of which could reasonably impact the cytosolic refractive index. Lipid droplets are specialized cell structures that contain lipid complexes within a phospholipid membrane, and are coated with proteins that form a shell on the droplet surface

(Le Lay & Dugail 2009). We investigated the intracellular lipid deposition in tissues sections using an optimized quantitative Oil Red O staining technique (Koopman *et al.* 2001) that allows individual droplets to be visualized within fibers.

A checkerboard pattern was detected in tissue sections where staining intensity was notably greater for some fibers (Figure 6A). A comparison with adjacent stained sections confirmed that fibers with higher lipid staining were pure Type I and pure Type II fibers. These same fibers had greater mitochondrial density, higher mitochondrial activity and longer fluorescent lifetimes. Quantitative analysis revealed a significant effect of age on intracellular lipid distribution. In young animals, much of the lipid was detected as a fine mist within individual fibers but in mid-age and old animals visibly larger droplets were detected (Figure 6A). Stained sections were imaged at 20x magnification and analyzed using particle-counting software where objects were categorized in bins according to size (pixel area) (Figure S4). To ensure that each individual object could be detected in a given field and to avoid digital merging of smaller objects, the very tiny mist-like droplets were set below the threshold of detection. There was a statistically significant effect of age on both the number and size of lipid droplets. Muscle sections from young animals had significantly fewer lipid droplets across all size categories (Figure 6B), and old animals had more large droplets than mid-aged animals.

Unexpectedly, the overall intensity of lipid staining in skeletal muscle sections from young, mid-age and old animals was not different (Figure 6C). Although total amounts of intracellular lipid were not altered with age, the amount of lipid stain sequestered in droplet form significantly increased with age. Lipid stain pixel area within each droplet size category was significantly lower in young animals, with mid-age and old animals differing from young animals in pixel area for all size categories and with each other for all but the smallest detectable droplets (Figure 6D). These data show that even though the total lipid amount is not different with age, the manner in which the lipid is stored within the fibers is different. Lipids are less accessible within larger droplets and the age-induced accrual of larger droplets could be indicative of reduced lipid turnover.

Discussion

We identified a shift in metabolism in rhesus skeletal muscle that occurs at a relatively early time point in the aging process and in advance of muscle mass loss. The optical methods used for autofluroescent detection have advantages over traditional biochemical metabolic characterization methods in that they are non-invasive, can be done on intact sections and tissues, and provide a quantitative readout of both fluorescence intensity and chemistry changes that are correlated with metabolism. Our initial analysis detected a significant reduction in the fluorescent lifetime of metabolic cofactors NADH and FAD in middle-aged animals that suggested a major shift in the metabolic status of muscle fibers. This altered metabolic state was associated with increased levels of FAD. A complementary biochemical analysis of NAD revealed that levels of free NADH were elevated and NAD^+:NADH redox ratio was lower confirming a change in NAD related metabolism. Using more traditional immunohistological and histochemical techniques we detected changes in fiber type distribution and a reduction in mitochondrial activity providing further evidence for a shift in metabolism in middle age prior to sarcopenia onset. Further investigation revealed that PGC-1α subcellular localization was impaired with age, and the predicted downstream effect of reduced PGC-1α activity on lipid storage and utilization was also observed.

The heterogeneity of cell type in skeletal muscle presents several challenges for the study of aging: first, the fiber types are metabolically distinct; second, the distribution of fibers changes with age and metabolic characteristics are altered; and third, the response to aging is

not equivalent among fibers. Our previous work on an independent longitudinal rhesus monkey study showed that the rate of decline in muscle mass was reflected in the atrophy of fibers expressing Type II myosin isoform (McKiernan *et al.* 2012). Unlike the prior study that did not distinguish between Type II and MMF, here we measured CSA for both pure Type II and MMF. MMF fibers appear to be more resilient to age-associated atrophy than pure Type II fibers. In addition, MMF are significantly larger than Type II fibers, especially in old animals. These data suggest that retention of a greater proportion of MMF, such as that observed in CR animals, would be beneficial in preserving muscle mass. The ability of fibers to switch type in response to changes in innervation or energetic demand has long been appreciated. Although it is currently unclear what drives the mid-age fiber type distribution shift, one possible explanation is that it is an adaptation to age-associated changes in metabolism.

Studies in isolated mitochondria, homogenized tissues and permeabolized fibers consistently find a decline in mitochondrial activity (Short *et al.* 2005; Figueiredo *et al.* 2009); however populations of mitochondria are mixed and there is disagreement about the extent to which isolation of mitochondrial contributes to changes in mitochondrial activities (Picard *et al.* 2010). Some of these challenges can be overcome by *in situ* studies using tissue sections. One remaining challenge stems from the nature of mitochondrial activity assays, in which maximal capacity is measured. These assays are conducted under substrate saturating conditions and reflect what mitochondria can do, but not what they are doing *in vivo*. This may be relevant for the mixed myosin fibers identified in this study. Maximal activity was lower for MMF but did not change with age. This raises the possibility that mitochondria from this hybrid fiber are not diminished in energetic capacity but differ in how oxidative phosphorylation takes place.

Changes in fiber type-specific myosin isoform and in mitochondrial energy metabolism point to PGC-1α regulated pathways in the metabolic transition at mid-age. Although overall levels of PGC-1α protein did not change with age, the changes in mitochondrial energy metabolism are consistent with a decline in PGC-1α activity with age. Immunohistological detection of PGC-1α indicates that its localization to the nucleus is impaired with age, suggesting a possible mechanism for diminished PGC-1α activity. The NAD dependent deacetylase SIRT1 is an activator of PGC-1α (Nemoto *et al.* 2005; Rodgers *et al.* 2005; Amat *et al.* 2009) that can also regulate PGC-1α cellular distribution (Anderson *et al.* 2008). The lower NAD:NADH ratio detected in mid-age is predicted to negatively influence SIRT1. Attempts to measure levels of SIRT1 in tissue homogenates were not successful; however, levels of NAMPT were lower in tissue from old animals. NAMPT is a key enzyme in the NAD salvage pathway that positively regulates SIRT1 activity in skeletal muscle in mice (Fulco *et al.* 2008). A decline in NAMPT would be predicted to lower SIRT1 activity, which would negatively influence PGC-1α localization and activity. The finding that subsarcolemmal mitochondria were more sensitive to the impact of age is of interest because this population of mitochondria is known to be most responsive to changes in PGC-1α activity (Benton *et al.* 2008).

The underlying basis for the age-associated metabolic changes is unclear. One possibility is a change in energetic demand. An earlier study of rhesus monkeys of equivalent age to this study cohort showed that energy expenditure declines with age and there is a significant decline in physical activity (Ramsey *et al.* 2000). In aged animals (>23 years), time at rest is increased and measures of both vertical and horizontal movement are significantly lower. This overall reduction in physical output would be predicted to influence skeletal muscle mitochondrial activity and lipid utilization. The influence of energetic demand on skeletal muscle at mid-age is less clear (13–17 years). Animals rest more but energy expenditure is not changed at this stage and lean mass is not lower. There is a reduction in horizontal but

not vertical movement; however, because the mid-age animals are significantly heavier it is difficult to assess a change in energetic demand. Our data demonstrate that muscle from mid-age animals is metabolically distinct from that of aged animals indicating that response to activity may not be equivalent. In humans there is a breakpoint at ~52 years of age where physical activity and activity energy expenditure is independent of age in younger but not in older subjects (Speakman & Westerterp 2010). An alternate explanation is that changes in muscle metabolism and composition at mid-age precipitate changes in physical activity. Indeed studies of obese humans support this idea, where muscle composition rather than muscle mass is an indicator of muscle weakness and subsequent physical impairment (Stenholm *et al.* 2008).

We propose that the changes in NAD metabolism that we detect in mid-age and old rhesus skeletal muscle are directly linked to changes in mitochondrial energy metabolism. This shift is predicted to have far reaching consequences, influencing expression of structural genes, lipid fuel utilization, and processes regulated by redox. Given the influence of muscle metabolism on systemic homeostasis (Canto & Auwerx 2009), interventions to preserve muscle metabolism and function are likely to yield significant benefits for multiple age-associated conditions that have a basis in metabolic dysfunction.

Experimental procedures

Animal care and tissue procurement

All animal protocols were carried out at the Wisconsin National Primate Research Center (WNPRC) with the approval of the Institutional Animal Care and Use Committee of the Graduate School of the University of Wisconsin, Madison.

For the aging study, animals were part of the WNPRC colony of rhesus macaques (Colman *et al.* 2005). Animals were group housed and fed *ad libitum*. The following age groups were represented: Young, age 6- 9 years, n=5, five males; Mid-age, age 14–15 years, n=4, two males and two females; Old, age 28–30 years, n=5, three males and two females. For all but two animals, samples of *vastus lateralis* were procured during necropsy with tissue isolation and preparation occurring immediately upon expiration. Specimens were procured by biopsy for two of the five young animals.

For the calorie restriction experiment (~30% food restriction) *vastus lateralis* biopsies specimens were obtained from animals involved in the WNPRC longitudinal study (Colman *et al.* 2009). Control (n=4, age 27–30 years) and CR (n=6, 27–32 years) male animals were housed individually and had been participating in the study for ~18 years. Further details are provided in the Supporting Information.

Multiphoton imaging

Autofluorescent detection and lifetime imaging was conducted using a multiphoton workstation at the University of Wisconsin Laboratory for Optical and Computational Instrumentation (LOCI, www.loci.wisc.edu). Details are provided in the Supporting Information. The selection of fields was unbiased except for the following exclusions: where fibers were not present in transverse section, where the epimysium was enlarged, where there were folds in the specimen. Fields with enlarged epimysium were avoided because of the autofluorescence properties of collagen polymers in gaps between fibers that would contribute to the fluorescence. For fluorescent intensity measures, the contribution from small amounts of collagen is negligible. For lifetime calculations any area containing collagen was excluded from the calculations. Details of biochemical detection of NAD, histochemistry, immunohistochemistry, histology, and western blot are provided in the Supporting Information.

Digital image capture and analysis

Unless otherwise the stained slides were imaged with a 20x objective in a Leica DM4000B microscope and photographed with a Retiga 4000R digital camera (QImaging Systems, Surrey, BC, Canada). Camera settings were optimized for each stain and for uniformity all images with were taken with identical settings, fixed light levels and fixed shutter speed. Images for Oil Red O lipid stained sections were captured within 24 hours of tissue processing. Quantitative image analysis was performed using ImagePro Plus 6.3.1.542 Software or Adobe Photoshop CS3 (Adobe Systems, San Jose, CA). Details specific to each stain are provided in the Supporting Information.

Statistical analysis

Rhesus monkeys are genetically heterogeneous. The statistical approach was optimized for each of the experiments. For routine analysis including western blot and biochemical detection of NAD the Students t-test was applied with a cut off of $p<0.05$.

Elsewhere the statistical approach was guided by the data set. For example, for fiber type distribution a Welch correction for the degrees-of-freedom (dfs) were applied to the analysis of variance (ANOVA) because of the extreme heterogeneity in the standard deviations across the age groups. Pairwise comparisons were made using the mean ranks from nonparametric Kruskal-Wallis test, and a pairwise Fligner-Policello for unequal variances. Semi-parametric regression using Generalized Estimating Equations (GEE) with exchangeable covariance structures was applied to account for the dependency in the data and to determine significant differences in fiber numbers across groups. For cytochrome c oxidase data applicable a linear mixed model was used to test differences in the groups. O'Brien's Test for Homogeneity of Variance performed on the un-clustered data to determine variability. Pairwise comparisons with Tukey-Kramer adjustments for multiple testing were applied to determine differences among groups. Lipid droplet count data were viewed as a mixture of Poisson distributions so zero-inflated Poisson and Negative Binomial distribution were evaluated as an offset variable. For the pixel area of the droplets a GEE was modeled with a Gamma distribution. Further details are provided in the Supporting Information.

Supplementary Material

Refer to Web version on PubMed Central for supplementary material.

Acknowledgments

The following lists the author contributions: PK, KE, RW, and RA designed the study, animal care and tissue procurement was performed by RC, data were generated by TP, MC, TE, MP, HB, RP, statistical analysis was performed by TMB, and the paper was written by BA and RA. We would like to acknowledge Scott Baum and Susan McKiernan for assistance with sample procurement. We also thank staff at LOCI for assistance with imaging instrumentation. Funding for this study was provided by NIA grant P01AG011915, NIH UL1RR025011, NIH R01CA13659, NIH R01AG037000, and the Department of Medicine, School of Medicine and Public Health UW Madison. The study was conducted with the use of resources and facilities at the William S. Middleton Memorial Veterans Hospital, Madison WI.

References

Amat R, Planavila A, Chen SL, Iglesias R, Giralt M, Villarroya F. SIRT1 controls the transcription of the peroxisome proliferator-activated receptor-gamma Co-activator-1alpha (PGC-1alpha) gene in skeletal muscle through the PGC-1alpha autoregulatory loop and interaction with MyoD. J Biol Chem. 2009; 284:21872–21880. [PubMed: 19553684]

Anderson RM, Barger JL, Edwards MG, Braun KH, O'Connor CE, Prolla TA, Weindruch R. Dynamic regulation of PGC-1alpha localization and turnover implicates mitochondrial adaptation in calorie restriction and the stress response. Aging Cell. 2008; 7:101–111. [PubMed: 18031569]

Bassel-Duby R, Olson EN. Signaling pathways in skeletal muscle remodeling. Annu Rev Biochem. 2006; 75:19–37. [PubMed: 16756483]

Benton CR, Nickerson JG, Lally J, Han XX, Holloway GP, Glatz JF, Luiken JJ, Graham TE, Heikkila JJ, Bonen A. Modest PGC-1alpha overexpression in muscle in vivo is sufficient to increase insulin sensitivity and palmitate oxidation in subsarcolemmal, not intermyofibrillar, mitochondria. J Biol Chem. 2008; 283:4228–4240. [PubMed: 18079123]

Bindewald-Wittich A, Han M, Schmitz-Valckenberg S, Snyder SR, Giese G, Bille JF, Holz FG. Two-photon-excited fluorescence imaging of human RPE cells with a femtosecond Ti:Sapphire laser. Invest Ophthalmol Vis Sci. 2006; 47:4553–4557. [PubMed: 17003452]

Bird DK, Eliceiri KW, Fan CH, White JG. Simultaneous two-photon spectral and lifetime fluorescence microscopy. Appl Opt. 2004; 43:5173–5182. [PubMed: 15473237]

Canto C, Auwerx J. PGC-1alpha, SIRT1 and AMPK, an energy sensing network that controls energy expenditure. Curr Opin Lipidol. 2009; 20:98–105. [PubMed: 19276888]

Colman RJ, Anderson RM, Johnson SC, Kastman EK, Kosmatka KJ, Beasley TM, Allison DB, Cruzen C, Simmons HA, Kemnitz JW, Weindruch R. Caloric restriction delays disease onset and mortality in rhesus monkeys. Science. 2009; 325:201–204. [PubMed: 19590001]

Colman RJ, McKiernan SH, Aiken JM, Weindruch R. Muscle mass loss in Rhesus monkeys: age of onset. Exp Gerontol. 2005; 40:573–581. [PubMed: 15985353]

Costford SR, Bajpeyi S, Pasarica M, Albarado DC, Thomas SC, Xie H, Church T, Jubrias SA, Conley KE, Smith SR. Skeletal Muscle NAMPT is Induced by Exercise in Humans. Am J Physiol Endocrinol Metab. 2009

de Magalhaes JP, Curado J, Church GM. Meta-analysis of age-related gene expression profiles identifies common signatures of aging. Bioinformatics. 2009; 25:875–881. [PubMed: 19189975]

Denk W, Strickler JH, Webb WW. Two-photon laser scanning fluorescence microscopy. Science. 1990; 248:73–76. [PubMed: 2321027]

Federico A, Manneschi L, Paolini E. Biochemical difference between intermyofibrillar and subsarcolemmal mitochondria from human muscle. Journal of Inherited Metabolic Disease. 1987; 10:242–246.

Figueiredo PA, Powers SK, Ferreira RM, Appell HJ, Duarte JA. Aging impairs skeletal muscle mitochondrial bioenergetic function. The journals of gerontology. Series A, Biological sciences and medical sciences. 2009; 64:21–33.

Fulco M, Cen Y, Zhao P, Hoffman EP, McBurney MW, Sauve AA, Sartorelli V. Glucose restriction inhibits skeletal myoblast differentiation by activating SIRT1 through AMPK-mediated regulation of Nampt. Dev Cell. 2008; 14:661–673. [PubMed: 18477450]

Jager S, Handschin C, St-Pierre J, Spiegelman BM. AMP-activated protein kinase (AMPK) action in skeletal muscle via direct phosphorylation of PGC-1alpha. Proc Natl Acad Sci U S A. 2007; 104:12017–12022. [PubMed: 17609368]

Koopman R, Schaart G, Hesselink MK. Optimisation of oil red O staining permits combination with immunofluorescence and automated quantification of lipids. Histochem Cell Biol. 2001; 116:63–68. [PubMed: 11479724]

Koves TR, Li P, An J, Akimoto T, Slentz D, Ilkayeva O, Dohm GL, Yan Z, Newgard CB, Muoio DM. Peroxisome proliferator-activated receptor-gamma co-activator 1alpha-mediated metabolic remodeling of skeletal myocytes mimics exercise training and reverses lipid-induced mitochondrial inefficiency. J Biol Chem. 2005; 280:33588–33598. [PubMed: 16079133]

Lakowicz JR, Szmacinski H, Nowaczyk K, Johnson ML. Fluorescence lifetime imaging of free and protein-bound NADH. Proc Natl Acad Sci U S A. 1992; 89:1271–1275. [PubMed: 1741380]

Le Lay S, Dugail I. Connecting lipid droplet biology and the metabolic syndrome. Prog Lipid Res. 2009; 48:191–195. [PubMed: 19303902]

Lexell J. Human aging, muscle mass, and fiber type composition. The journals of gerontology. Series A, Biological sciences and medical sciences. 1995; 50(Spec No):11–16.

Lin J, Wu H, Tarr PT, Zhang CY, Wu Z, Boss O, Michael LF, Puigserver P, Isotani E, Olson EN, Lowell BB, Bassel-Duby R, Spiegelman BM. Transcriptional co-activator PGC-1 alpha drives the formation of slow-twitch muscle fibres. Nature. 2002; 418:797–801. [PubMed: 12181572]

Lowell BB, Shulman GI. Mitochondrial dysfunction and type 2 diabetes. Science. 2005; 307:384–387. [PubMed: 15662004]

McKiernan SH, Colman R, Lopez M, Beasley TM, Weindruch R, Aiken JM. Longitudinal analysis of early stage sarcopenia in aging rhesus monkeys. Exp Gerontol. 2009; 44:170–176. [PubMed: 18983905]

McKiernan SH, Colman RJ, Aiken E, Evans TD, Beasley TM, Aiken JM, Weindruch R, Anderson RM. Cellular adaptation contributes to calorie restriction-induced preservation of skeletal muscle in aged rhesus monkeys. Exp Gerontol. 2012; 47:229–236. [PubMed: 22226624]

McKiernan SH, Colman RJ, Lopez M, Beasley TM, Aiken JM, Anderson RM, Weindruch R. Caloric restriction delays aging-induced cellular phenotypes in rhesus monkey skeletal muscle. Exp Gerontol. 2011; 46:23–29. [PubMed: 20883771]

Mootha VK, Lindgren CM, Eriksson KF, Subramanian A, Sihag S, Lehar J, Puigserver P, Carlsson E, Ridderstrale M, Laurila E, Houstis N, Daly MJ, Patterson N, Mesirov JP, Golub TR, Tamayo P, Spiegelman B, Lander ES, Hirschhorn JN, Altshuler D, Groop LC. PGC-1alpha-responsive genes involved in oxidative phosphorylation are coordinately downregulated in human diabetes. Nat Genet. 2003; 34:267–273. [PubMed: 12808457]

Nemoto S, Fergusson MM, Finkel T. SIRT1 functionally interacts with the metabolic regulator and transcriptional coactivator PGC-1{alpha}. J Biol Chem. 2005; 280:16456–16460. [PubMed: 15716268]

Noland RC, Koves TR, Seiler SE, Lum H, Lust RM, Ilkayeva O, Stevens RD, Hegardt FG, Muoio DM. Carnitine insufficiency caused by aging and overnutrition compromises mitochondrial performance and metabolic control. J Biol Chem. 2009; 284:22840–22852. [PubMed: 19553674]

Petersen KF, Dufour S, Befroy D, Garcia R, Shulman GI. Impaired mitochondrial activity in the insulin-resistant offspring of patients with type 2 diabetes. N Engl J Med. 2004; 350:664–671. [PubMed: 14960743]

Picard M, Ritchie D, Wright KJ, Romestaing C, Thomas MM, Rowan SL, Taivassalo T, Hepple RT. Mitochondrial functional impairment with aging is exaggerated in isolated mitochondria compared to permeabilized myofibers. Aging Cell. 2010; 9:1032–1046. [PubMed: 20849523]

Proctor DN, Sinning WE, Walro JM, Sieck GC, Lemon PW. Oxidative capacity of human muscle fiber types: effects of age and training status. J Appl Physiol. 1995; 78:2033–2038. [PubMed: 7665396]

Ramsey JJ, Laatsch JL, Kemnitz JW. Age and gender differences in bodycomposition, energy expenditure, and glucoregulation of adult rhesus monkeys. Journal of medical primatology. 2000; 29:11–19. [PubMed: 10870670]

Revollo JR, Grimm AA, Imai S. The NAD biosynthesis pathway mediated by nicotinamide phosphoribosyltransferase regulates Sir2 activity in mammalian cells. J Biol Chem. 2004; 279:50754–50763. [PubMed: 15381699]

Rodgers JT, Lerin C, Haas W, Gygi SP, Spiegelman BM, Puigserver P. Nutrient control of glucose homeostasis through a complex of PGC-1alpha and SIRT1. Nature. 2005; 434:113–118. [PubMed: 15744310]

Seligman AM, Karnovsky MJ, Wasserkrug HL, Hanker JS. Nondroplet ultrastructural demonstration of cytochrome oxidase activity with a polymerizing osmiophilic reagent, diaminobenzidine (DAB). J Cell Biol. 1968; 38:1–14. [PubMed: 4300067]

Sethi JK, Vidal-Puig AJ. Thematic reviewseries: adipocyte biology. Adipose tissue function and plasticity orchestrate nutritional adaptation. J Lipid Res. 2007; 48:1253–1262. [PubMed: 17374880]

Short KR, Bigelow ML, Kahl J, Singh R, Coenen-Schimke J, Raghavakaimal S, Nair KS. Decline in skeletal muscle mitochondrial function with aging in humans. Proc Natl Acad Sci U S A. 2005; 102:5618–5623. [PubMed: 15800038]

Skala MC, Riching KM, Gendron-Fitzpatrick A, Eickhoff J, Eliceiri KW, White JG, Ramanujam N. In vivo multiphoton microscopy of NADH and FAD redox states, fluorescencelifetimes, and cellular

morphology in precancerous epithelia. Proc Natl Acad Sci U S A. 2007; 104:19494–19499. [PubMed: 18042710]

Speakman JR, Westerterp KR. Associations between energy demands, physical activity, and body composition in adult humans between 18 and 96 yof age. Am J Clin Nutr. 2010; 92:826–834. [PubMed: 20810973]

Stenholm S, Harris TB, Rantanen T, Visser M, Kritchevsky SB, Ferrucci L. Sarcopenic obesity: definition, cause and consequences. Current opinion in clinical nutrition and metabolic care. 2008; 11:693–700. [PubMed: 18827572]

Tanaka F, Tamai N, Yamazaki I, Nakashima N, Yoshihara K. Temperature-induced changes in the coenzyme environment of D-amino acid oxidase revealed by the multiple decays of FAD fluorescence. Biophys J. 1989; 56:901–909. [PubMed: 2574999]

Uno H. Are-related pathology and bioscenescent markersin captive rhesus macaques. Age. 1997; 20:1–13. [PubMed: 23604287]

Wu Z, Puigserver P, Andersson U, Zhang C, Adelmant G, Mootha V, Troy A, Cinti S, Lowell B, Scarpulla RC, Spiegelman BM. Mechanisms controlling mitochondrial biogenesis and respiration through the thermogenic coactivator PGC-1. Cell. 1999; 98:115–124. [PubMed: 10412986]

Yan L, Rueden CT, White JG, Eliceiri KW. Applications of combined spectral lifetime microscopy for biology. Biotechniques. 2006; 41:249, 251, 253. passim. [PubMed: 16989084]

Zahn JM, Sonu R, Vogel H, Crane E, Mazan-Mamczarz K, Rabkin R, Davis RW, Becker KG, Owen AB, Kim SK. Transcriptional profiling of aging in human muscle reveals a common aging signature. PLoS Genet. 2006; 2:e115. [PubMed: 16789832]

Zierath JR, Hawley JA. Skeletal muscle fiber type: influence on contractile and metabolic properties. PLoS Biol. 2004; 2:e348. [PubMed: 15486583]

Zipfel WR, Williams RM, Christie R, Nikitin AY, Hyman BT, Webb WW. Live tissue intrinsic emission microscopy using multiphoton-excited native fluorescence and second harmonic generation. Proc Natl Acad Sci U S A. 2003; 100:7075–7080. [PubMed: 12756303]

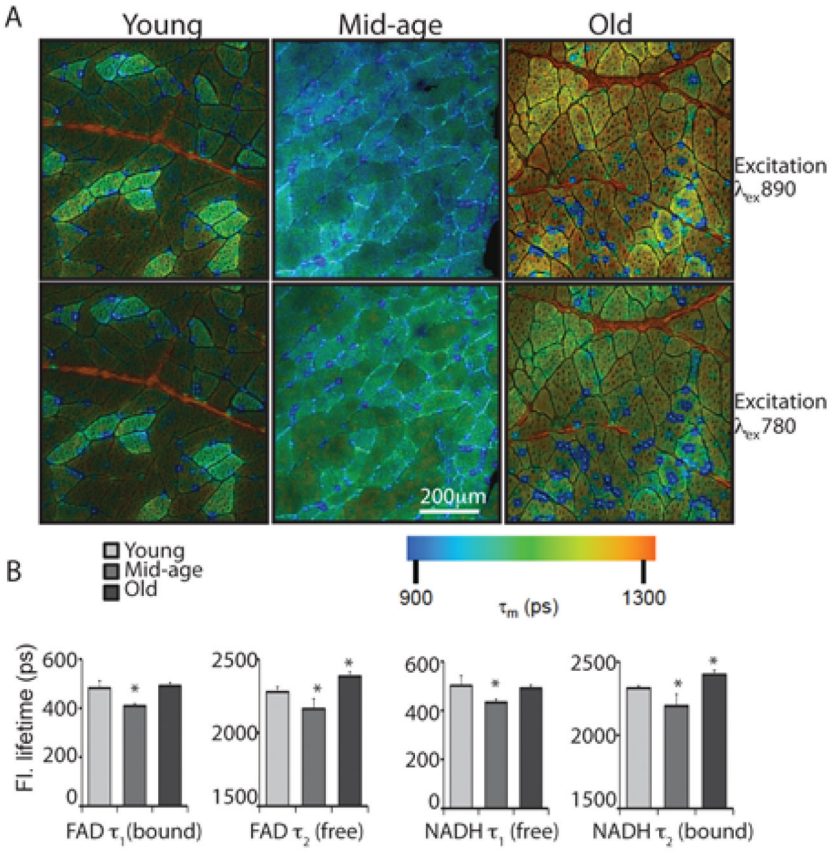

Figure 1.

Age impacts the fluorescent lifetime of endogenous fluorophores in skeletal muscle. (A) Sections of vastus lateralis prepared from young (8 years old), mid-age (15 years old) and old (28 years old) rhesus monkeys were imaged using excitation wavelengths of 890nm and 780nm. Pulsed laser excitation and high discrimination photon counting were used to generate aggregate decay curves from which lifetime was calculated. The weighted average of both short and long decay components (t_m) in pico seconds were color mapped according to the scale shown. (B) Individual components of the exponential decay function for FAD and NADH in tissues from young (6–9 years, n=4, 10 images), mid-age (15–16 years, n=3, 11 images), old (28–30 years, n=4, 15 images) animals are shown in pico seconds as average ±SEM. (* $p<0.05$).

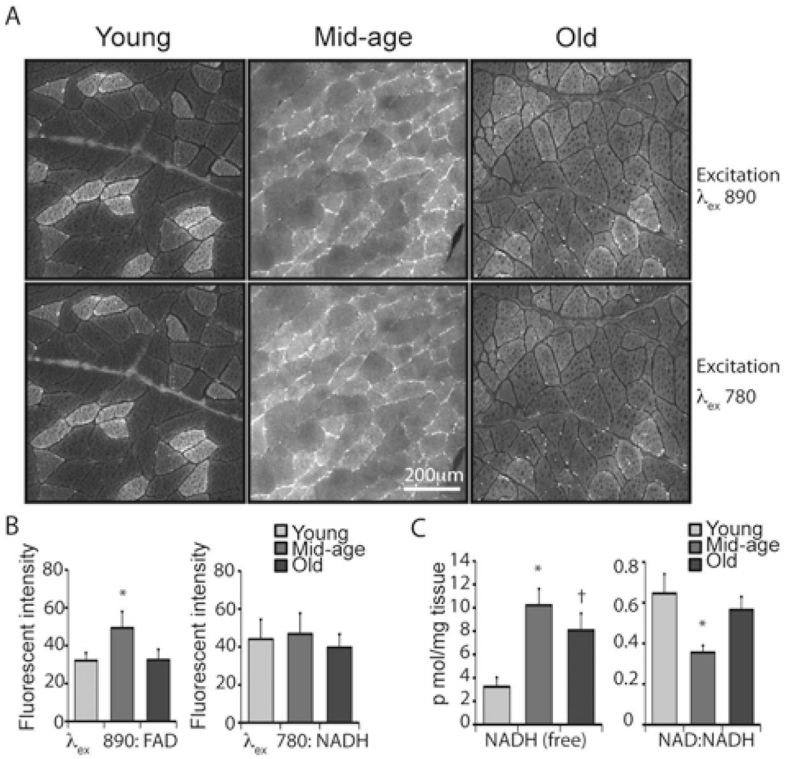

Figure 2.

Levels of FAD and NADH are elevated in mid-age skeletal muscle and redox ratio is shifted. (A) Fluorescent intensity imaged using excitation wavelengths of 890nm and 780nm in sections of vastus lateralis prepared from young (8 years old), mid-age (15 years old) and old (28 years old) rhesus monkeys. (B) Fluorescent intensity was calculated from images captured with indicated excitation wavelengths; young (6–9 years, n=4, 10 images), mid-age (15–16 years, n=3, 11 images), old (28–30 years, n=4, 15 images) shown as average ±SEM. (C) Levels of NAD and NADH were determined in vastus lateralis tissue homogenate from n=4 animals per age group shown as average ±SEM. (* $p<0.05$).

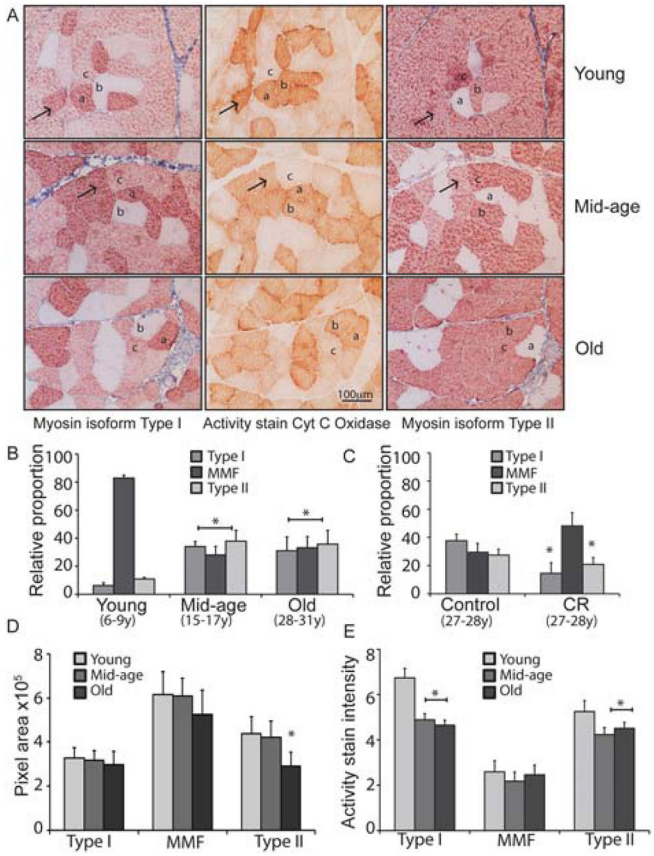

Figure 3.

Structural and metabolic profiles of skeletal muscle fibers are altered in mid-age monkeys. (A) Immunohistolochemical detection of Type I (left) or Type II (right) specific myosin isoforms, and histochemical detection of cytochrome c oxidase activity (center) in adjacent vastus lateralis sections from young (6 years old), mid-age (15 years old) and old (28 years old) animals. (B) Relative proportion of individual fiber types in tissues from young (6–9 years, n=5), mid-age (15–16 years, n=4), old (28–30 years, n=5) (avg >450 fibers per animal) shown as average ±SEM. (C) Relative proportion of individual fiber types in tissues from Control (n=4) and CR (n=5) fed animals (age 27–32) shown as average ±SEM (average >500 fibers per animal). (D) Cross-sectional area in fibers from young (6–9 years, n=3), mid-age (15–16 years, n=3), old (28–30 years, n=3) animals shown as average ±SEM. (E) Quantitation of cytochrome c oxidase activity stain intensity within individual fibers from young (n=5), mid-age (n-3) and old (n=3) animals (average 31 fibers per fiber type per animal) shown as average ±SEM. (* $p<0.05$).

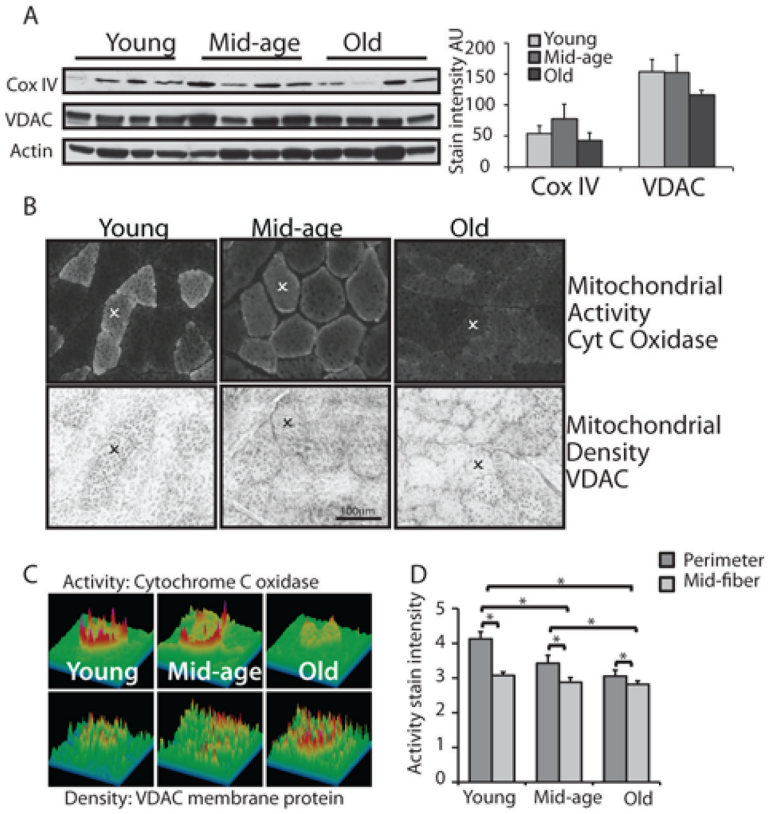

Figure 4.

Mitochondrial subcellular organization within muscle fibers is progressively lost with age. (A) Detection of cytochrome c oxidase subunit IV of the mitochondrial ETS and voltage dependent anion channel membrane protein in tissue homogenates from vastus lateralis in young (6–9 years), mid-age (15–16 years), old (28–30 years). Quantitation of western blot detection of cytochrome c oxidase and VDAC normalized to actin (n=4) shown as average ±SEM. (B) Histochemical and immunohistochemical detection of cytochrome c oxidase activity and VDAC in tissues sections from young (8 years), mid-age (14 years), and old (29 years) animals. Identical fibers are identified in upper and lower panels (χ). (C) Surface plots of stain intensity within matched individual fibers from (B). (D) Quantitation of cytochrome c oxidase activity stain in perimeter and mid-fiber regions of Type I fibers from young (6–9 years, n=5), mid-age (15–16 years, n=3), old (28–30 years, n=3), shown as average ±SEM. (* $p<0.05$).

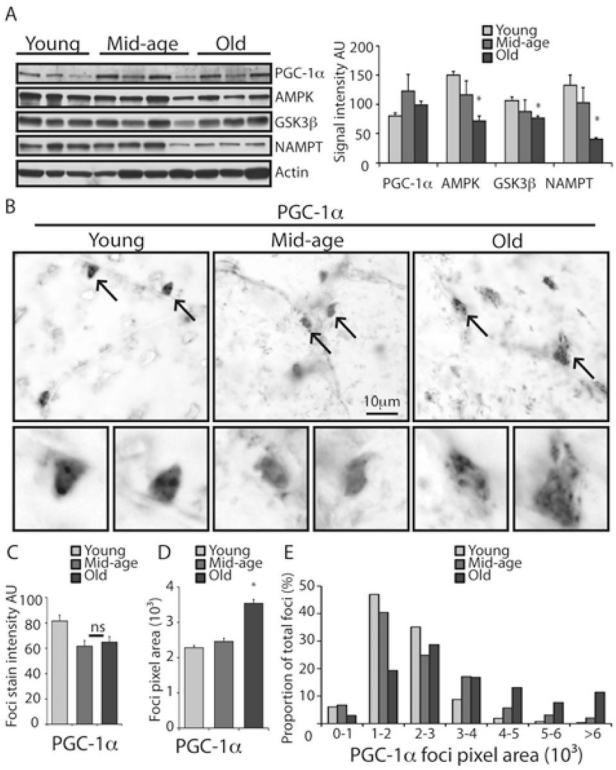

Figure 5.

Deregulated nuclear accumulation of PGC-1α in skeletal muscle fibers with age. (A) Western blot detection of PGC-1α and associated regulating proteins in tissue homogenates from young (6–9 years, n=3), mid-age (14–15 years, n=4), old (28–30 years, n=3) monkeys. Pixel intensity for each protein normalized to actin is shown as average ±SEM. (B) Immunohistochemical detection of PGC-1α in tissue sections from young (8 years), mid-age (14 years) and old (28 years) animals. (C) Quantitation of PGC-1α stain area within individual foci in muscle fibers (average ~300 foci per age group) from young (6–9 years, n=5), mid-age (15–16 years, n=3), old (28–31 years, n=3) shown as average ±SEM. (D) PGC-1a foci pixel area in the same tissues (E) Pixel area distribution of PGC-1α stained foci. (* $p<0.05$)

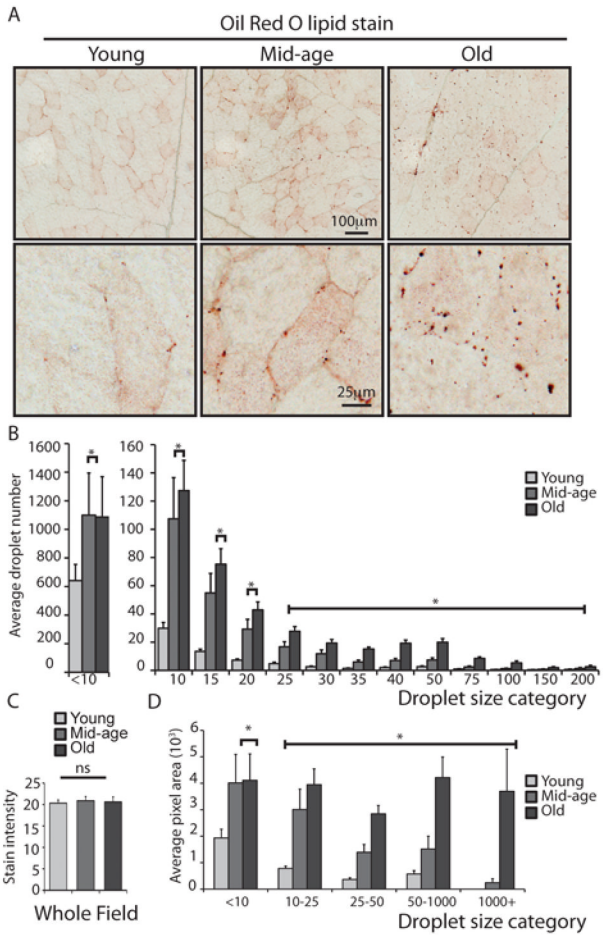

Figure 6.

Age-associated change in intracellular lipid storage in skeletal muscle fibers. (A) Lipids detected in skeletal muscle tissue sections from young (8 years), mid-age (14 years) and old (28 years) rhesus monkeys using an optimized Oil Red O staining procedure (top panels), zoomed image showing individual droplets within fibers (bottom panels). (B) Numbers of droplets of indicated size detected in 20x field (n=4–7) in sections from young (6–9 years, n=4), mid-age (14–15 years, n=4), old (28–30 years, n=4) monkeys shown as average ±SEM. (C) Total stain intensity was measured in above sections shown as average ±SEM. (D) Average pixel area attributed to droplets calculated for the indicated grouped droplet size categories shown as average ±SEM. (* $p<0.05$)